(Received 13 November 2025, Accepted 8 December 2026, Scheduled 1 March 2026)

On the Performance of CRLH Antenna Loaded with AMC Reflector for Direct Antenna Modulation Process

Yahiea Alnaiemy[1], Mariam Q. Abdalrazak[2], Zainab Salam[3], and Taha A. Elwi[4, *]

[1] *Department of Computer Science, College of Science, University of Diyala, Diyala, Iraq*
[2] *Technical College of Engineering/Al-Bayan University, Baghdad, Iraq*
[3] *Department of Electrical Engineering, Mustansiriyah University, Baghdad, Iraq*
[4] *Department of Automation and Artificial Intelligence Engineering College of Information Engineering at Al-Nahrain University, Baghdad, Iraq*

ABSTRACT: This paper introduces an innovative antenna design for direct antenna modulation (DAM) applications in the 5G sub-6 GHz band. The antenna has a composite right/left-handed (CRLH) structure, an electromagnetic bandgap (EBG) made of Hilbert inclusions, and an artificial magnetic conductor (AMC) reflector. The AMC reflector reflects light with no phase shift at the design frequency, boosting forward gain to a maximum of 20 dBi at 5.59 GHz and reducing back lobes. One important new idea is to use integrated light-dependent resistors (LDRs) for photonic reconfiguration. This lets one change the antenna's impedance and resonant characteristics in real time. Changing LDR states dynamically changes the antenna's gain in real time. For example, at 5.5 GHz, it can go from 10.11 dBi to 19.85 dBi. This makes it possible to do direct amplitude modulation without any outside modulators. Experimental results validate the effective implementation of DAM, demonstrating quantifiable alterations in channel capacity and bit error rate (BER) associated with varying antenna gain states. The suggested system shows a practical, adaptable antenna solution for modern adaptive communication systems.

1. INTRODUCTION

Due to the increased demand for wireless communication systems, it became essential to develop adaptive, inexpensive antennas with high performance, including multi-bands and good gain, specifically for 5G systems [1, 2]. Recently, different ways have emerged to design miniature antennas through metamaterial loadings [3]. Metamaterial (MTM) structures are manufactured by utilizing either a transmission line or a resonance approach. The transmission line approach consists of a CRLH-structure characterized by a combination of right-handed (RH) and left-handed (LH) transmission properties. In contrast, the resonant approach consists of split ring resonators (SRRs) and complementary split ring resonators (CSRRs) [4].

The transmission line structure was characterized by zero-order resonance, which was a very important feature of MTM-antennas when the resonance of the antenna becomes distinct and independent of the length of the transmission line [5]. Nevertheless, as a result of the MTM compact design, it produced low gain, narrow bandwidth, and low radiation efficiency, in addition to design complexity due to the use of Vertical Interconnect Access (VIA) that restricts the use of metamaterials in various wireless applications [6] to overcome the aforementioned problems and improve the performance of the antenna. Different methods were used by including metamaterials with the antenna structure, such as EBG, Perfect Electric Conductor (PEC), AMC reflector, and MTM substrate loadings [7]. However, these multi-layer antennas show large sizes, narrow bandwidth, low efficiency, and low gain, in addition to the existence of VIA that complicates the fabrication process of the antenna [8–10]. Hence, these antennas are unsuitable for applications that require high efficiency with low complexity.

In this work, an AMC reflector is combined with a CRLH-TL-based antenna, to enhance the gain, radiation efficiency, as well as the beamwidth of 5G systems. AMC structures with antennas have recently attracted the interest of scientific communities due to their distinctive characteristic [11]. In this section, some of the recent research in the field of interest is presented [12]. A dual-band antenna with a composite right-left-handed transmission line (CRLH) and an artificial magnetic conductor (AMC) was proposed. The radiator antenna, designed with AMC-MS, achieves a gain enhancement of 6.46 and 7.12 dBi for the two frequency bands centered at 3.27 and 5.11 GHz, respectively [13]. A heart-shaped antenna with a 3×3 AMC ground plane was designed; in the presence of AMC, it achieved a peak gain of 5.86 dBi at the WiMAX band, representing a 225% increase in gain. Similarly, at the WLAN band, the antenna achieves a gain of 5.33 dBi, which represents a 141% increase in gain [14]. A coplanar waveguide (CPW)-fed monopole antenna with an AMC structure was proposed, and dual-band operation was achieved and extended from (2.37–2.5) GHz and (4.45–4.9) GHz, with a peak gain of 5 dBi and 7.5 dBi, respectively [15]. A multi-band antenna supported by an AMC was presented. The AMC unit cell comprises four metallic nested rings (FMNRs) and four lumped capacitors. The antenna with AMC achieves a gain im-

* Corresponding author: Taha Ahmed Elwi (taelwi82@gmail.com).

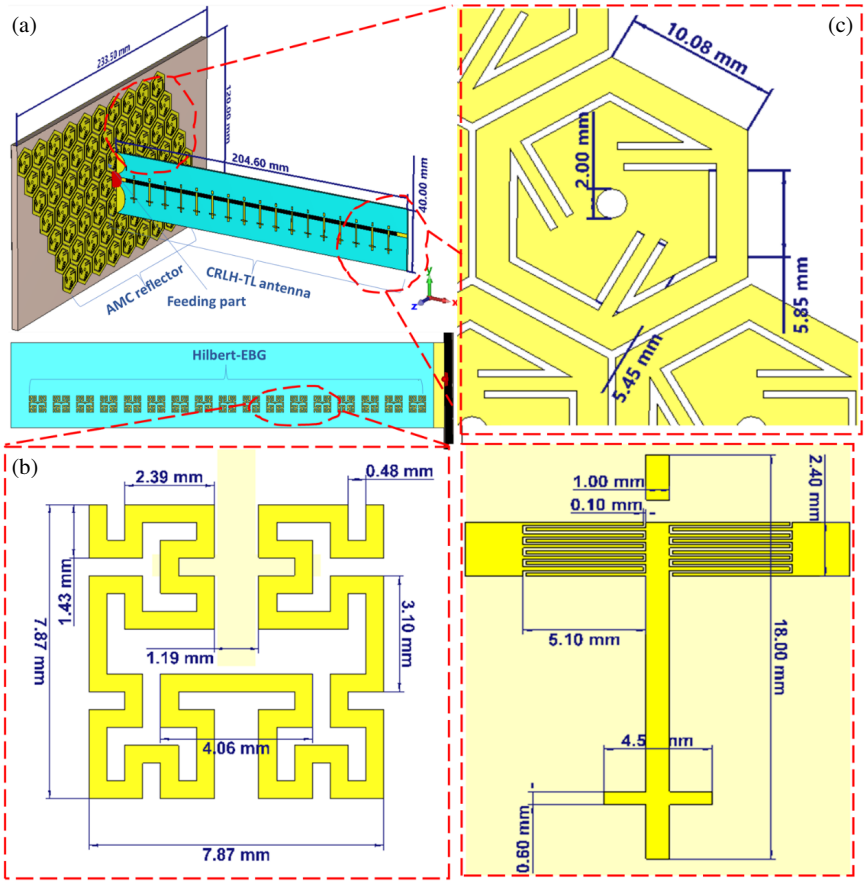

FIGURE 1. Antenna geometry. (a) 3D view, (b) EBG view, and (c) AMC view. Note: All dimensions are in mm scale.

provement of 4.93, 5.92, 5.54, and 4.95 dB at frequencies of 2.45, 3.5, 4.6, and 5.8 GHz, respectively. This makes it appropriate for applications such as WLAN, WiMAX, and 5G mobile communication systems [16]. A dual-band and dual-polarized antenna was proposed. The antenna includes two components: dual-band dipole antennas with $\pm 45°$ polarization and an AMC reflector. The antenna operates within the frequency ranges of 2.31–2.61 and 5.13–5.50 GHz. A 4×4 AMC reflector is utilized to achieve a suitable unidirectional radiation pattern. A gain of 7.24 dBi and 8.93 dBi is achieved in low and high-frequency bands, respectively [17]. A wideband slotted patch antenna with resistive loading was suggested for use in ground-penetrating radar (GPR) applications. The suggested design is supported by an optimized reflector consisting of a periodic array of square loop elements, improving the antenna's directivity and gain. It achieves a maximum gain of 7 dBi over a wide frequency range of 0.6 to 4.6 GHz [18]. An antenna with a metamaterial-based planner monopole design has been suggested. In order to achieve unidirectional radiation, a 5×5 artificial magnetic conductor (AMC) surface is employed as a back cavity. This surface is placed beneath the antenna at a height of $\lambda_o/12$ mm. The antenna achieves a maximum gain of 8 dBi in the lower frequency band (3.1–8.3 GHz) and upper-frequency band (8.4–14 GHz), making it appropriate for wideband wireless applications [19]. A linearly polarized antenna-based AMC is proposed [20]. An array-based AMC layer was suggested to minimize the dimension of the dipole [21]. The AMC unit includes a circular patch featuring four groups of symmetrical slots. An increase in the gain of 9.9 dBi is achieved, reducing the profile from 0.190 to 0.120.

In this paper, a CRLH-TL antenna structure loaded with an AMC reflector was proposed for 5G applications. The proposed design is constructed from a C_{IDC} coupled in parallel to L_{TS} to realize a gain bandwidth product enhancement. To reduce the effect of via losses, Hilbert inclusions are introduced as inclusions to the antenna back panel. The proposed antenna consists of seventeen symmetrical T-shaped CRLH unit cells loaded with the third-order Hilbert curve structure and fed with 50 Ω radio frequency (RF) port. A 7×10 reflector array is placed in front of the proposed antenna to realize a gain bandwidth product enhancement. The proposed antenna with an AMC reflector realizes a maximum gain of 20 dBi at 5.59 GHz with $S_{11} \leq -6$ dB.

2. ANTENNA GEOMETRY

Figure 1 displays the schematic view and fabricated model of the CRLH-TL-based antenna. The suggested antenna model consists of two layers. The 1st-layer is the CRLH-TL antenna depicted in Figure 1(a), and the 2nd-layer is the AMC reflector used to improve the antenna performance as shown in Figure 1(b). The CRLH-TL is fabricated on an RF4 substrate with a relative permittivity (ε_r) of 4.3, thickness of 1.57 mm, and loss tangent ($\tan \delta$) of 0.0033.

The proposed antenna is a new combination of several metamaterial ideas that were designed to work in the 5G sub-6 GHz spectrum with high gain and the ability to be reconfigured. The main part of the antenna is a CRLH-TL structure. This structure changes the way that physical size and electrical performance are related in antenna design. The CRLH paradigm allows operation beyond standard size constraints due to its distinctive dispersion properties that facilitate both right-handed (RH) and left-handed (LH) propagation modes. The LH behavior is made possible by a carefully designed interdigital capacitor (C_{IDC}) that provides series capacitance and a T-stub inductor (L_{TS}) that provides shunt inductance. Together, these two parts create a negative refractive index region that is necessary for miniaturization. The CRLH structure is important because it supports resonances that follow the formula $\beta_n = n\pi/L$. The zero-order resonance ($n = 0$) happens regardless of the physical length L, which lets the antenna work on multiple bands while keeping its size small. This mathematical relationship shows how the antenna can work at 5.5 GHz without following the usual $\lambda/2$ dimensional rules. This is a big step forward in making antennas smaller for 5G applications that do not require a lot of space.

One of the main problems with traditional CRLH designs is that they lose too much power through vias. Adding a third-order Hilbert fractal structure as an EBG element solves this problem. To balance the capacitive effect of the ground plane, traditional implementations need vias to create the necessary inductive effect. However, these vias cause large ohmic losses that lower gain and efficiency. The Hilbert fractal method reduces this lossy via with a smart distributed network that is printed on the backplane of the substrate.

The equation $c = [p\varepsilon_0(1+\varepsilon_r)/\pi]\cosh^1[(p+g)/g]$ [12] describes the physics behind this EBG design. In this equation, p is the width of the EBG cell, g the space between cells, and ε_r the substrate permittivity. This equation gives a mathematical definition of the capacitive gap between two Hilbert cells that are next to each other. Together, these cells make a high-impedance surface that stops surface waves from spreading. The capacitive reactance, which is given by $xc = 1/(2\pi f cgap)$ [9], creates a filtering effect that changes with frequency. This effect reduces unwanted surface currents while allowing efficient radiation at the design frequency. The Hilbert fractal's self-similar, space-filling shape makes the effective electrical length as long as possible in a small area. It increases the parasitic capacitance and inductance that naturally come from the interaction with the substrate. This new method gets rid of via losses and improves surface wave suppression, resulting in measured gain improvements of 2–4 dBi across the operational band compared to traditional via-based designs.

An Artificial Magnetic Conductor (AMC) reflector with a 7×10 array of hexagonal unit cells and star-shaped slots helps improve performance even more. The AMC works by reflecting waves that are in phase with each other. This is mathematically expressed as $\angle\Gamma_{\mathrm{AMC}}(f_0) = 0°$ at the design frequency of 5.5 GHz. This zero-phase reflection condition changes the way the antenna radiates by turning what would normally be a 180° out-of-phase reflection from a Perfect Electric Conductor (PEC) ground into constructive interference in the forward direction. The AMC works like a magnetic "soft" boundary that cuts down on back lobes and boosts front-directed radiation. This gives it a 4 dBi gain improvement and a maximum gain of 20 dBi. The hexagonal unit cell shape with slots placed in the right places makes sure that surface currents are evenly spread out, which keeps the zero-phase condition across a wide range of frequencies. It means that performance is always good across all 5G operational bands.

An innovative photonic control system using Light-Dependent Resistors (LDRs) built into the T-stub elements makes it possible for the antenna to be reconfigured. The LDR's resistance drops from about 1 MΩ to 100 Ω when it is lit up. This changes the electrical length of the T-stub inductor and the local impedance distribution across the CRLH structure. This change in impedance changes the antenna's resonance frequency in real time. It also lets one steer the beam by using selective illumination patterns across multiple LDRs, with a range of $\pm 5°$. The optical switching mechanism works without complicated bias networks or mechanical parts, which makes it easier to change things while still keeping high radiation efficiency. The mathematical link between the intensity of the incoming light and the resistance of the LDR makes it possible to continuously tune the antenna, which can then be used for both frequency reconfiguration and beam scanning. This makes the antenna adaptable to changing channel conditions in dynamic 5G environments.

This all-encompassing design strategy — combining CRLH miniaturization through zero-order resonance, EBG surface wave suppression through designed capacitive gaps, AMC phase-engineered reflection, and optical impedance tuning — creates a system where each part fixes a problem while improving the system as a whole. The mathematical equations that govern each part show a strict physics-based design process that goes beyond trial-and-error optimization to engineering based on basic principles. The resulting antenna has a better gain-bandwidth product while still being able to be reconfigured and small enough to fit in with modern 5G systems' needs for high performance, adaptability, and form factor efficiency in sub-6 GHz applications.

3. RESULTS AND PARAMETRIC STUDY

This part explains the antenna design process and the fundamental parameters for achieving the final results. The design was analyzed and simulated using the Computer Simulation Technology Microwave Studio (CST MWS) based on the finite integration technique. For this, we applied the simulation study to monitor the S_{11} and gain spectra for each step as follows.

3.1. C_{IDC} Effects

For good estimation, the design of C_{IDC} can be calculated according to Equation (1) from [13]:

$$C_{\mathrm{IDC}} \approx (N-1)\varepsilon_0\varepsilon_{eff}\frac{L}{g} \tag{1}$$

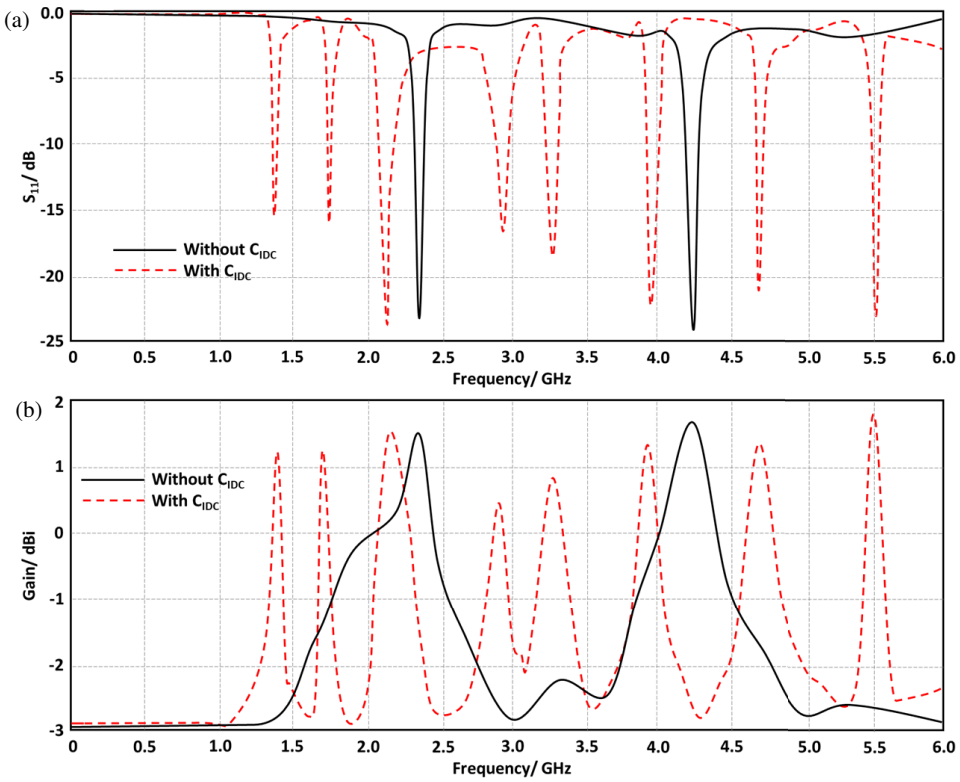

FIGURE 2. C_{IDC} effects. (a) S_{11}, (b) realized gain.

where N is the number of fingers, ε_{eff} the effective permittivity, L the figure length, and g the gap between fingers. For this, the relative simulation with CST MWS is adopted with and without introducing the proposed C_{IDC} based on five fingers. We started from a printed monopole antenna as a microstrip line printed on a substrate to be compared to the one with C_{IDC} as seen in Figure 2 in terms of S_{11} and gain spectra. It is found that the C_{IDC} introduction realized multiple frequency resonances with limited gain due to the effects of energy storing [4].

3.2. T-Stub Effects

To match the effects of the introduced C_{IDC}, a T-stub is introduced to minimize the effects of energy stored at the same frequency resonance as given by the design equation (2) based on [12]:

$$l_{\text{T\_stub}} = \frac{L_{\text{target}} c}{Z_0 \sqrt{\varepsilon_{eff}}} \tag{2}$$

where $l_{\text{T\_stub}}$ is the stub inductance, L_{target} the stub length, Z_o the input impedance, and c the speed of light.

For this, the proposed antenna performances in terms of S_{11} and gain spectra with and without T-stub structure performance are compared to each other as presented in Figure 3. Several shifts and changes are observed in the obtained S_{11} spectra. However, the antenna gain is found to be increased significantly after introducing the T_stub. Such enhancement in the antenna gain is attributed to the effects of introducing the T_stub that eliminated the storing part due to C_{IDC}.

3.3. Unit Cell Periodicity Effects

To test the effect of periodicity, a parametric study is applied to realize the effect of the unit cell number increase on the antenna performance. For this, we increased the unit cell number from one unit cell to 17 unit cells with a step of 4-unit cells increase with each attempt. Each unit cell is based on a CRLH inclusion and backed with EBG fractal from the back. It is found that increasing the number of unit cells increases the antenna gain significantly with an observed enhancement in the antenna bandwidth as shown in Figure 4. Such enhancement in the antenna gain is attributed to that the increased periodicity led to excellent matching between the antenna electromagnetic aperture impedance and the intrinsic impedance of the space with minimum reflection [18]. However, observed enhancements in the antenna bandwidth is achieved due to the increase in the surface current paths because of the increase of unit cell number.

3.4. AMC Reflector Effects

Before characterizing the effects of the reflector introduction on the antenna performance, we applied a study on the proposed AMC unit cell characterizations. For this, we evaluated the unit cell characteristics in terms of reflection phase change with frequency as shown in Figure 5. In this work, the proposed hexagonal unit cell is characterized after passing through three attempts to arrive at the optimal design at which the reflection coefficient reaches zero at 5.5 GHz. Therefore, we started with a hexagonal unit cell design, then, a hexagonal unit cell with an internal trace is etched from the unit cell conductor, and the

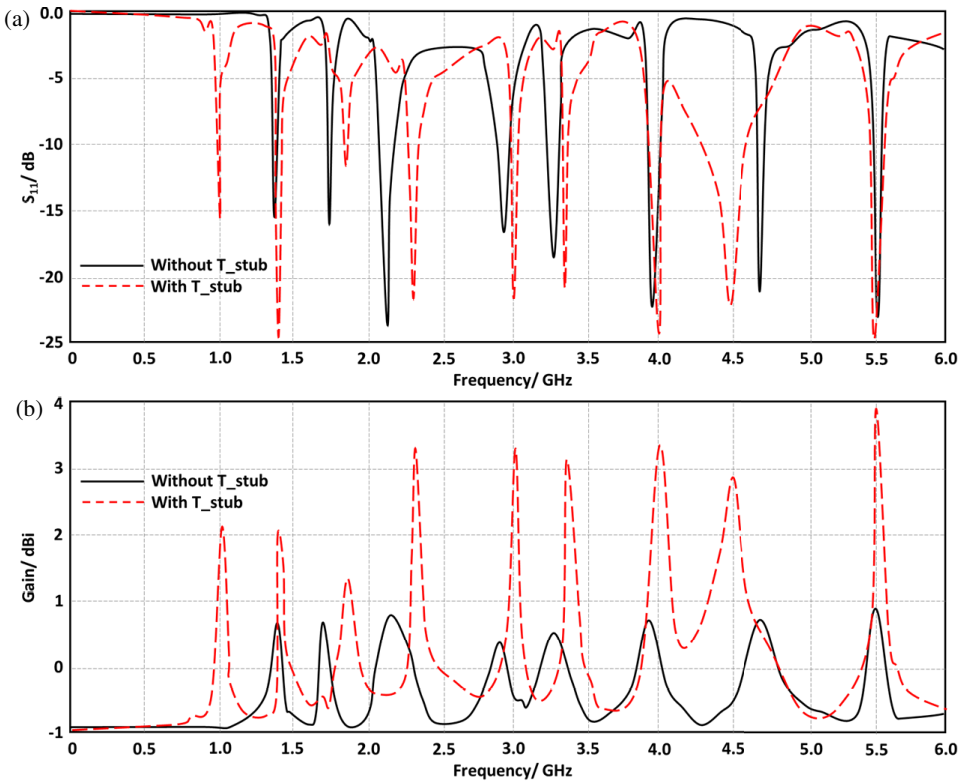

FIGURE 3. T_stub effects. (a) S_{11}, (b) realized gain.

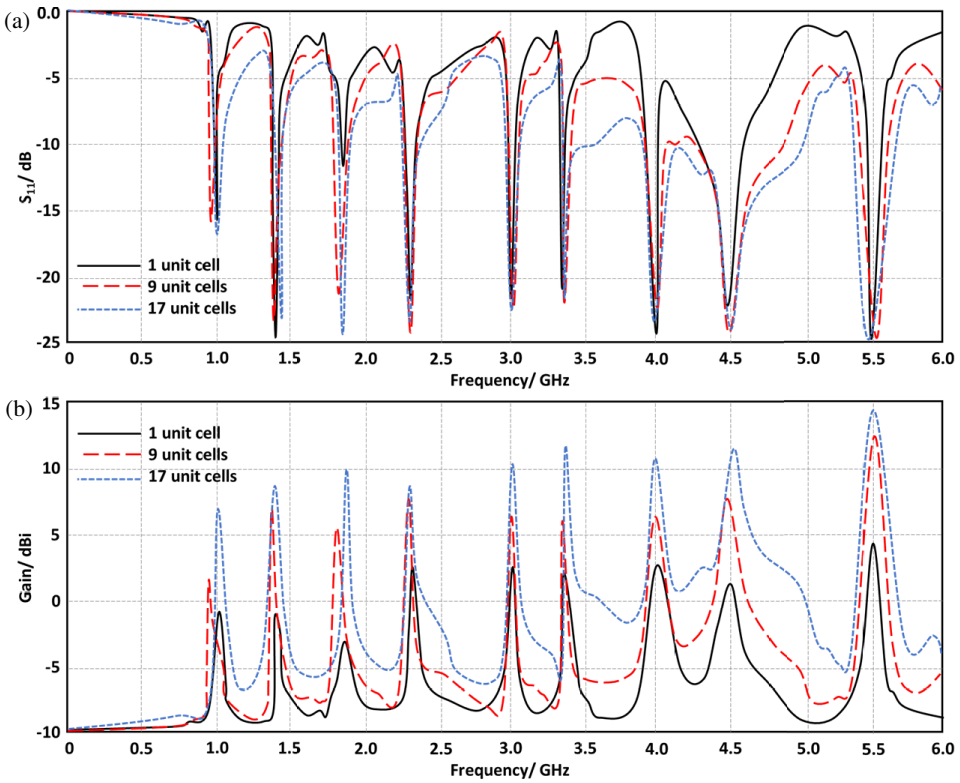

FIGURE 4. Unit cell number effects on: (a) S_{11}, (b) realized gain.

third design with via structure introduction to the unit cell center. It is found that the proposed unit cell reaches zero reflection coefficient at 5.5 GHz when the third design is considered as seen in Figure 5. Thus, the third design is considered for the reflector design. Accordingly, the resulting schematic design based on the resulting unit cell for this reflector was extended to a 7×10 array as shown in Figure 1(c) to occupy an effective area about $179.5 \times 123.91\,\text{mm}^2$.

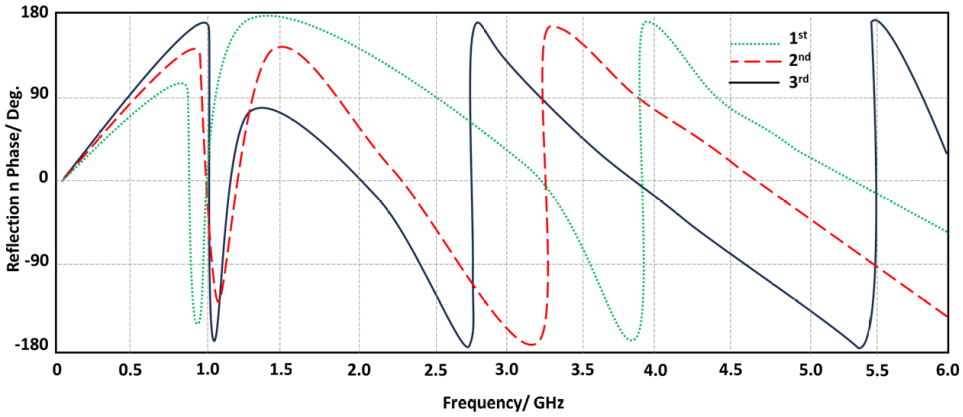

FIGURE 5. The AMC performance in terms of phase spectrum.

After introducing the proposed AMC reflector array to the proposed antenna, significant enhancements in the antenna performance are achieved to reach the antenna gain about 20 dBi with the total bandwidth enhancement about 3 GHz. The location of the proposed AMC reflector with respect to the antenna is considered at the back focal length from the antenna back side to reflect the backscattered radiations toward the front lobe direction. The integration of the proposed AMC reflector array yields a substantial enhancement in the antenna's radiative performance. A maximum realized gain of approximately 20 dBi is achieved, accompanied by a significant improvement in the impedance bandwidth, extending over 3 GHz within the sub-6 GHz 5G band. This improvement is primarily attributed to the AMC's engineered electromagnetic response. The reflector is positioned at a calculated back focal distance from the antenna's radiating plane. This specific placement is critical, as it ensures that backscattered radiation, which would normally be lost or degraded as back lobes, is reflected with a zero-phase shift ($\angle\Gamma \approx 0°$) at the design frequency. This in-phase reflection constructively interferes with the primary forward wave, effectively redirecting energy from the rear hemisphere into the main lobe. Consequently, this mechanism simultaneously boosts forward gain, suppresses back-lobe radiation, and improves the front-to-back ratio, transforming the pattern into a highly directive, unidirectional beam suitable for long-range 5G links. Here are the three key design equations for the AMC reflector starts from the basic phase-matching [3]:

$$2\beta d + \phi_{\text{AMC}} = 2\pi \tag{3}$$

where β is the phase shift, d the distance between the antenna and AMC reflector, and ϕ_{AMC} the inherent phase difference of the AMC layer. To ensure the reflected waves added constructively in our case ϕ_{AMC} = zero at 5.5 GHz, the back focal length (BFL) (for minimal phase error) can be realized based on [3]:

$$\text{BFL} \approx \frac{R^2}{2\varepsilon_r(n \times m)\lambda_0} \tag{4}$$

where R is the reflector radius; λ_0 is the wavelength at 5.5 GHz; $n \times m$ are the AMC array indexes in our case (7×10); and the relative permittivity in terms of ε_r minimizes phase variation across the AMC array. These equations optimize the gain and directivity by positioning the AMC at an ideal back focal point. According to that, if we evaluate BFL from Equation (4), about 1.95 mm can be found. As seen in Figure 6, the evaluated antenna performances before and after the AMC introductions are presented.

3.5. Gain Control

Adaptive antenna gain value is achieved through changing the switching process on the antenna structure for the antenna LDR. Table 1 shows the variation in the antenna gain that is achieved with respect to the switching process 5.5 GHz. The variation in the antenna gain is attributed to the change in the main lobe value only without any change in the antenna direction as seen in Figure 7. Such gain changes are attributed to the effects of resistance increases that reduce the gain value dramatically with respect to the switching process and increase the accumulative resistance [16].

TABLE 1. AMC structure gain control.

Case	Input sequence	Gain/dBi
1	0000000000000000	19.85
2	10101010101010101	15.05
3	1111111111111111	10.11

4. EXPERIMENTAL VALIDATION AND DISCUSSIONS

The proposed antenna, characterized by highly complex geometrical features with minimum line widths and gaps of 0.1 mm, was fabricated on an FR-4 substrate ($\varepsilon_r = 4.4$, $\tan\delta = 0.02$, thickness = 1.6 mm) using a high-resolution photolithographic and wet chemical etching process. The fabrication was performed using an LPKF ProtoLaser S4 direct laser imaging system combined with an LPKF Contac S4 wet processing unit to ensure precise pattern transfer and repeatability. Initially, the copper-clad substrate was chemically cleaned using isopropyl alcohol and deionized water for 3 minutes, followed by nitrogen drying to eliminate surface contamination and improve photoresist adhesion. A 35 µm copper layer was coated with a 25 µm dry-film photoresist and laminated at 115°C for 2 minutes under controlled pressure. The antenna layout was then transferred by a direct laser exposure at 375 nm for approxi-

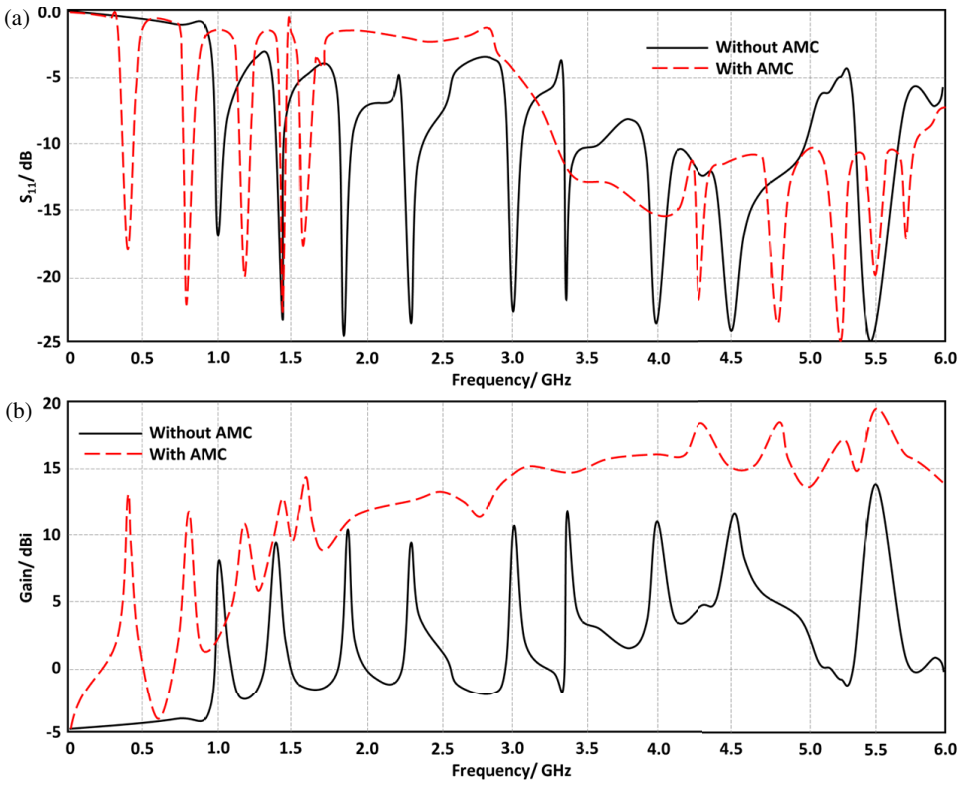

FIGURE 6. AMC array influence on: (a) S_{11} and (b) gain spectra.

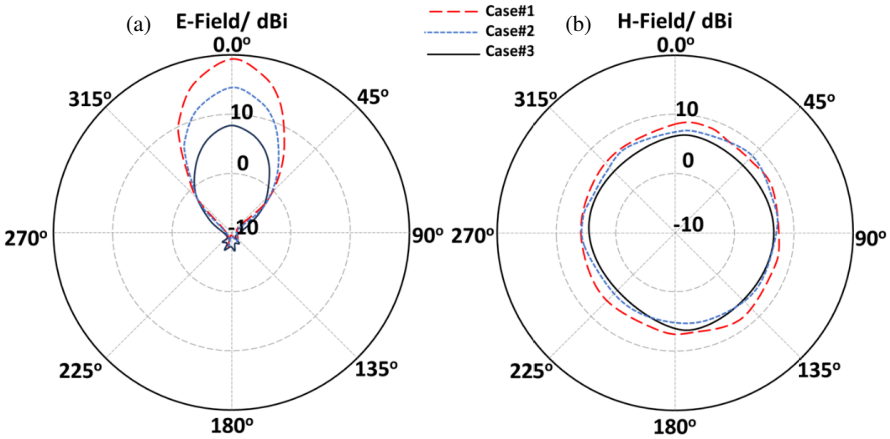

FIGURE 7. The AMC structure beam-scan at 5.5 GHz.

mately 120 seconds, enabling sub-100 µm resolution and accurate reproduction of fine geometrical details. The exposed substrate was developed in a 1% sodium carbonate solution for 60 seconds to remove unexposed resist regions.

Chemical etching was conducted using a temperature-controlled ferric chloride solution maintained at 40°C, with continuous agitation to ensure uniform copper removal. The etching time was carefully monitored and limited to 4 minutes to prevent undercutting and preserve the 0.1 mm critical dimensions. The remaining photoresist was stripped in a dilute sodium hydroxide solution for 2 minutes, followed by thorough rinsing in deionized water and air drying. Optical microscopy inspection with 10× and 50× magnification was used to verify dimensional fidelity and edge definition. The resulting antenna exhibited well-defined features with dimensional deviations below ±10 µm, making the fabrication process suitable for high-frequency, miniaturized, and densely patterned antenna structures.

The fabricated antenna, see Figure 8, is installed on a rotating table inside a special radio frequency (RF) chamber and connected to a spectrum analyzer to measure the radiation intensity. A vector network analyzer (37347A) is used for measuring the antenna parameters as shown in Figure 8. For frequency reconfiguration, visible light is used to lighten the antenna LDR for ON, and in case OFF, the LDR switches are covered with black table.

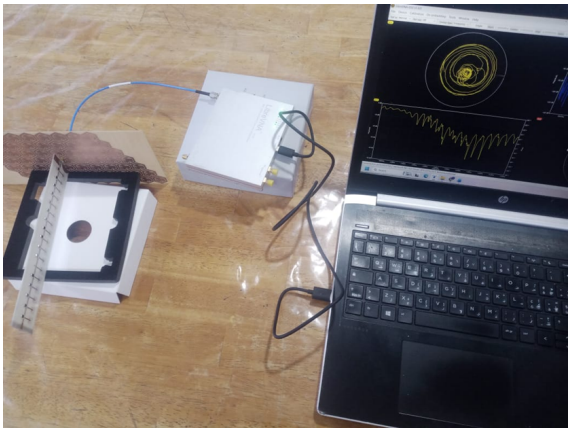

FIGURE 8. The antenna measurements performance.

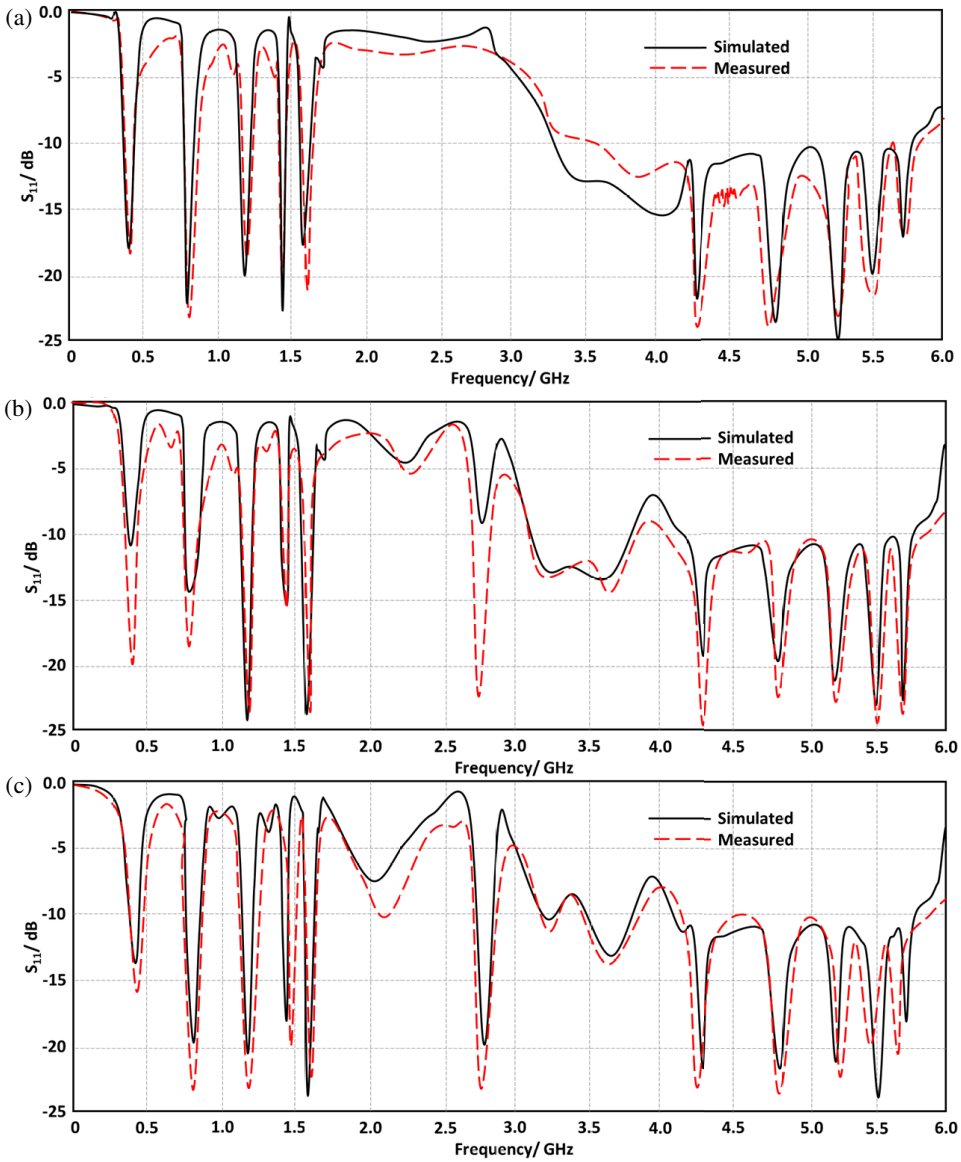

FIGURE 9. The measured S_{11} spectra for the considered switching configurations of the proposed cases from Table 1 as: (a) 00000000000000000, (b) 10101010101010101, and (c) 11111111111111111.

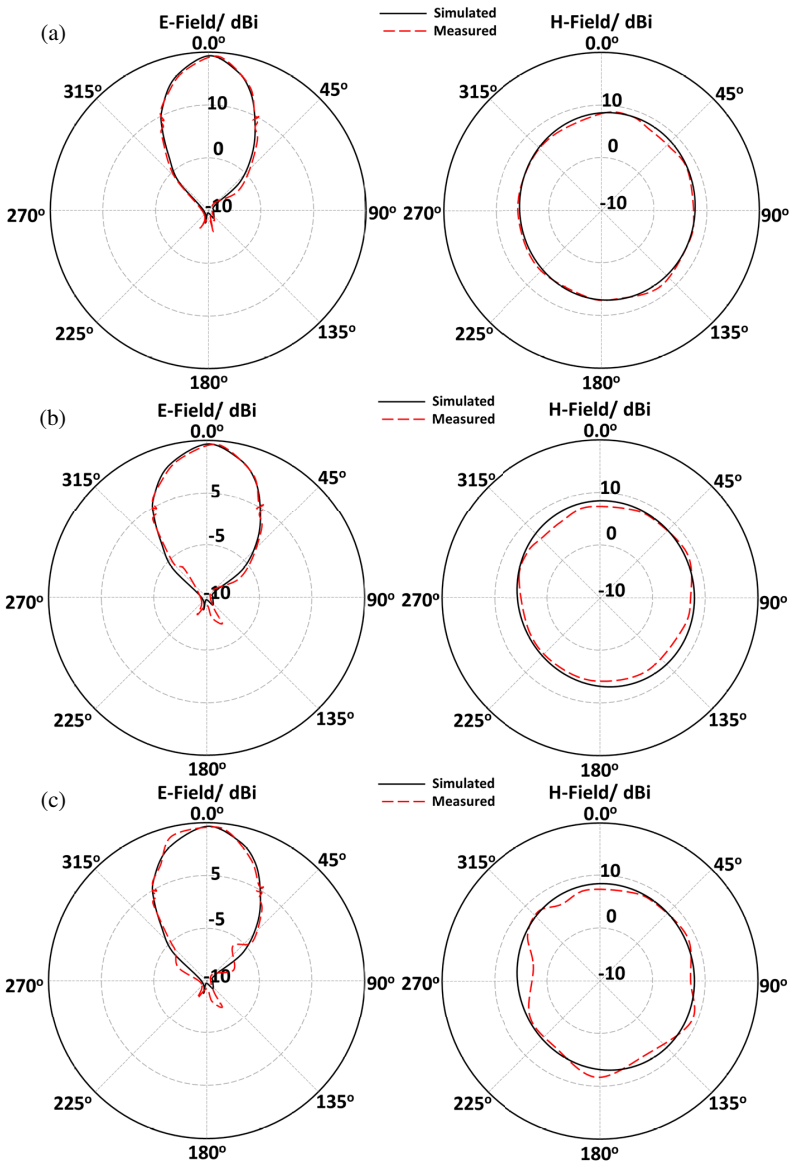

FIGURE 10. Antenna radiation patterns in the E-plane and H-plane at 5.5 GHz according to: (a) 00000000000000000, (b) 10101010101010101, and (c) 11111111111111111.

The measured S_{11} spectra of the fabricated prototype are compared to their identical ones from the simulation as seen in Figure 9. The considered cases in Table 1 during the switching process are measured accordingly and compared to their relative simulation results. We found an excellent agreement between the measured and simulated results. Nevertheless, the antenna bandwidth is found to be affected by the switching process that changes the matching impedance of the frequency resonances. However, the frequency band around 5.5 GHz is found to stay below 5.5 GHz, which motivated us to keep this frequency for the next measurement process.

Next, the main beam direction of the proposed antenna radiation patterns in the E- and H-planes of the fabricated prototype are tested at three considered cases in Table 1 at 5.5 GHz as shown in Figure 10. Experimentally, the numerical results in Table 1 and Figure 7 are validated. Such observations due to the effects of the AMC reflector based via inclusions that dominate the beam direction to main lobe direction in the endfire of the antenna sight as seen in Figure 10.

The proposed antenna undergoes evaluation through a drive test model in a real-world system-based local network and is compared to a standard commercial industrial antenna operating within the same frequency band at 5.5 GHz, as illustrated in Figure 11. We discovered that the proposed antenna achieves a substantial improvement compared to the standard one. The measured channel performance is based on distance and includes received signal (Rx), Reference Signal Received Quality (RSRQ), Reference Signal Received Power (RSRP), and Signal to Interference and Noise Ratio (SINR). Figure 11 shows a comparison of the channel metrics. The solid lines for the proposed antenna and dashed lines for the standard antenna show how performance changes with distance. The data shows that the proposed antenna design performs better than all other designs in terms of Rx Level, RSRP, RSRQ, and SINR. This was

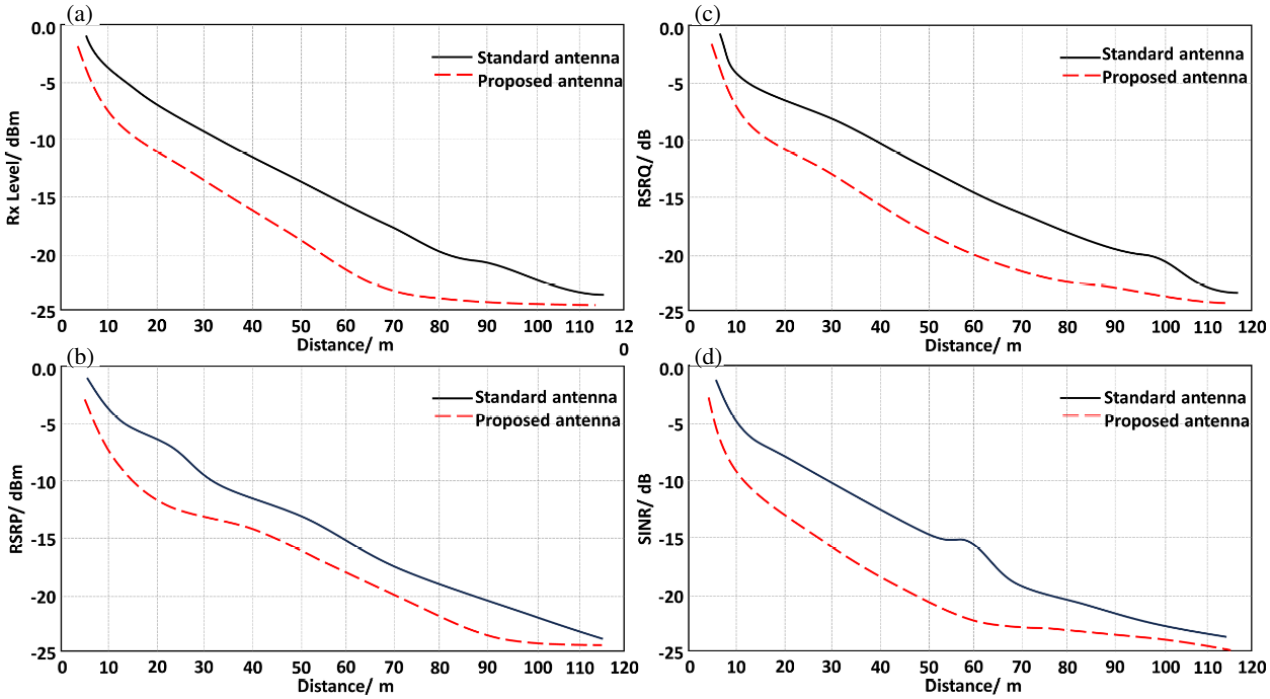

FIGURE 11. The drive test measurements in terms of (a) Rx, (b) RSRP, (c) RSRQ, and (d) SINR.

because its electromagnetic properties have been improved in terms of received power and antenna gain. The most obvious thing to notice is that the signal strength has become better. The Friis transmission equation says that received power (P_r) is directly related to the gain of the receiving antenna (G_r).

$$P_r \propto P_t G_t G_r \left(\frac{\lambda}{4\pi d}\right)^2 \tag{5}$$

The suggested antenna has a consistently higher RSRP. For instance, at a distance of 25 meters, the proposed antenna records an RSRP of about -70 dBm, while the standard antenna drops to -78 dBm. This 8 dB difference suggests that the proposed antenna has a higher realized gain and radiation efficiency. It means that the impedance matching is better (lower S_{11} values), which means that the most power is sent from the air interface to the receiver circuitry instead of being lost to reflection or dielectric losses in the antenna substrate.

Quality of the signal and direction (SINR and RSRQ). The SINR (Signal-to-Interference-plus-Noise Ratio) and RSRQ results show that the antenna can block interference. The proposed antenna has a SINR of 18 dB at 40 meters, which is much better than the standard antenna's 11 dB.

From a physics point of view, this improvement is probably due to better radiation pattern characteristics, such as lower Sidelobe Levels (SLL) and a higher Front-to-Back Ratio. In a "drive test" setting with many reflections, an antenna with high sidelobes picks up noise and clutter from directions that are not on-axis. The proposed antenna focuses its beam toward the source by suppressing these sidelobes. It makes the signal component (S) stronger than the interference (I) and noise (N). Also, the stability of the RSRQ suggests that polarization has gotten

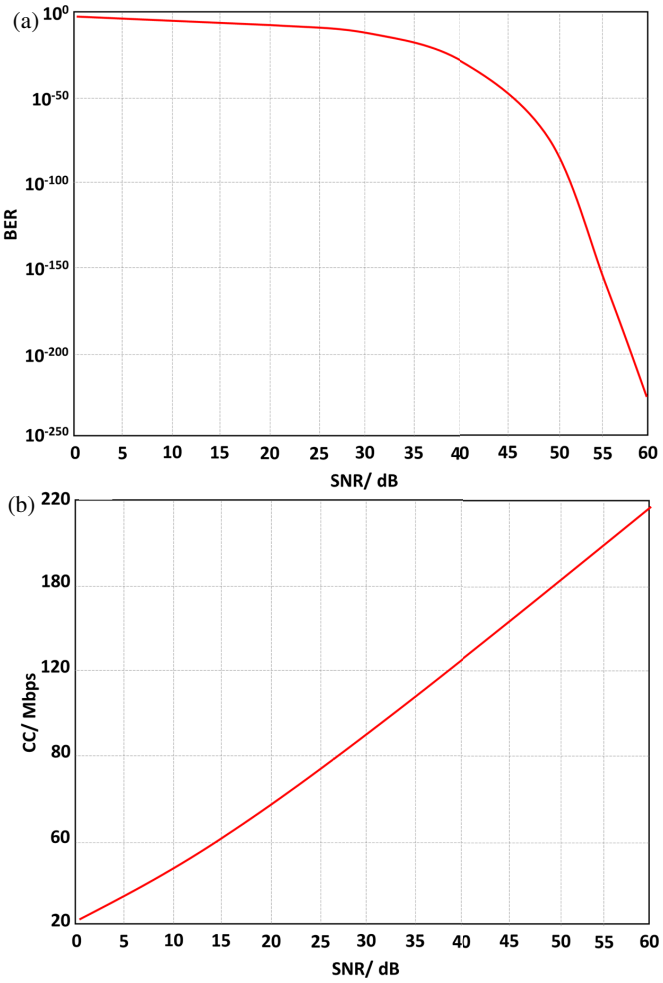

FIGURE 12. Channel performance in terms of: (a) BER and (b) CC.

TABLE 2. The comparison of the AMC reflector antenna with the relative interest.

Ref.	Technique used	Frequency	Max. gain	Via	Substrate
[22]	slots patch+AMC	3.26–3.73, 4.68–5.05	15.7	12	F4B
[23]	planar inverted-F antenna+AMC	4.8–6.7	7.6	—	RT 5880
[24]	bowtie dipoles+AMC	3.1–3.8, 4.4–5	8.2	2	FR-4
[25]	monopole+AMC	2.38–2.7, 3.28–5.8	7.1	—	FR-4
[26]	dipole+AMC	4.48–7	8.2	1	FR-4
[27]	monopole+AMC	3–5.09	8.7	—	R 4003C
[28]	slotted a bow-tie antenna+AMC	2.4–2.7, 3.4–3.8, 5.17–6.45	10.5	—	Arlon 880
[29]	cross-dipole antenna+AMC	3.14–5.32	15	—	FR-4
[30]	cross dipole+AMC	3.3–3.6, 4.8–5.0	9.28	4	RO4350B
[31]	dipole+AMC	3.26–6.02	8.4	—	Taconic TLT
[32]	slots-patches+AMC	1.7–2.5, 5.1–5.6	7.2	—	FR4
Proposed design	CRLH+Hilbert+AMC	5.51–5.66	20	—	Taconic RF-43

better purity or Cross-Polarization Discrimination (XPD). The signal quality quickly goes down if the standard antenna has polarization mismatch loss as the vehicle moves. The solid line on the proposed antenna stays stable above -10 dB, which means that it works well to reduce the effects of polarization mismatch and multipath fading that are common at 5.5 GHz.

Next, the direct antenna modulation (DAM) process is conducted based on the obtained results from the antenna measurements in terms of gain changes and frequency of operation as shown in Figure 12. The M-ary DAM analysis gives us numbers that show important performance trade-offs, which are important for system design. The analysis shows that for a 16-PSK system working at 5.5 GHz with 20 dBm transmitting power and 20 MHz bandwidth at a distance of 100 m in free space, the channel capacity is the highest at 95.3 Mbps with an antenna gain of about 20 dBi. To get this capacity, though, the SNR needs to be higher than 25 dB, which means that the BER needs to be lower than 10^{-5}. When the SNR is less than 10 dB, the BER drops quickly to about 0.1, which makes it impossible to communicate reliably. The SNR-BER relationship is easy to see: at 15 dB SNR, 16-PSK gets a BER of 2.3×10^{-4}, while the simpler Quadrature Phase Shift Keying (QPSK) ($M = 4$) gets a BER of 1.8×10^{-6} at the same SNR, which is almost two orders of magnitude better. This shows that phase modulations lose 3 dB–4 dB for every time M is doubled. Throughput calculations show that 16-PSK works the best at 15 dB–20 dB SNR, and at 18 dB SNR, it can reach 64 Mbps, which is 67% of the theoretical capacity because of error correction overhead.

The effects on the environment are significant: in cities, 12 dB–15 dB more transmitting power is needed to match free-space performance, and in buildings, 8 dB–10 dB more power is needed to make up for wall penetration losses. The noise figure contribution of 5 dB lowers the effective SNR by about 30%. This shows how important it is to design low-noise receivers. Most of the time, throughput efficiency is the highest around $M = 16$, with 3.2 bits/Hz spectral efficiency at 20 dB SNR. For QPSK, it is 2 bits/Hz, and for 64-PSK, it is 4 bits/Hz (which needs 28 dB SNR for the same BER). These numbers give clear rules for how to balance modulation order, power budget, and environmental constraints when real systems are built. The results clearly show that the best M-ary DAM design needs a careful analysis of the trade-offs among spectral efficiency, power efficiency, and environmental robustness.

Table 2 summarizes a comparison with the most recent dissertation; the proposed design provides a higher gain than the other designs, in addition to the ability for beam-scan, gain control, and frequency reconfiguration. This research emphasizes the significance of the high performance of the proposed antenna in wireless communication, specifically enhancing gain control with AMC reflector and CRLH structure for 5G applications. The proposed design offers high gain, compactness, and back scattering reduction capabilities. Driving tests reveal essential performance indicators such as SNR, RSRP, and Channel Quality Indicator (CQI) over a 250 m radius, highlighting unique propagation characteristics useful for mobile network planning in both rural and urban settings. The results validate the antenna's operation under varying channel conditions, demonstrating strong signal integrity. The study underscores the co-design of antennas and channels to enhance propagation capacities and suggests future exploration of massive multiple-

input multiple-output (MIMO) and AI-assisted beamforming to boost coverage and efficiency in next-gen communication systems.

5. CONCLUSION

For direct antenna modulation (DAM) in the 5G sub-6 GHz band, a high-gain, reconfigurable antenna based on a CRLH structure and an AMC reflector has been designed and tested. Adding a Hilbert-based EBG structure cut down on surface wave losses, and the zero-phase AMC reflector improved forward radiation, reaching a peak gain of 20 dBi. The addition of light-dependent resistors (LDRs) made it possible to change the antenna's performance without using electronics. The antenna's gain was dynamically controlled across multiple discrete states by changing the LDR switching patterns. This made it possible for the antenna to work as a variable-gain element in a DAM scheme. Experimental modulation tests validated that fluctuations in antenna gain directly affected system-level performance metrics, including channel capacity and Bit Error Rate (BER), thereby confirming the viability of the proposed design for amplitude-based modulation. This work proposes a promising, mechanically straightforward antenna solution for adaptive and reconfigurable wireless systems utilizing direct antenna modulation.

REFERENCES

[1] Elwi, T. A., F. Taher, B. S. Virdee, M. Alibakhshikenari, I. J. G. Zuazola, A. Krasniqi, A. S. Kamel, N. T. Tokan, S. Khan, N. O. Parchin, *et al.*, "On the performance of a photonic reconfigurable electromagnetic band gap antenna array for 5G applications," *IEEE Access*, Vol. 12, 60 849–60 862, 2024.

[2] Elwi, T. A., H. H. Al-Khaylani, W. S. Rasheed, S. A. Al-Salim, M. H. Khalil, L. A. Ali, O. A. Tawfeeq, S. T. Al-Hadeethi, D. Ali, Z. S. Muqdad, S. Özbay, and M. M. Ismael, "On the performance of metamaterial based printed circuit antenna for blood glucose level sensing applications: A case study," *Infocommunications Journal*, Vol. XVI, No. 1, 56–63, Mar. 2024.

[3] Majeed, A. M., T. A. Elwi, Z. A. A. Hassain, J. Kumar, and A. E. Saleem, "Orbital angular momentum-based slot array antenna for modern applications," *Journal of Engineering and Sustainable Development*, Vol. 28, No. 3, 375–383, 2024.

[4] Al-Saegh, A. M., F. Taher, T. A. Elwi, M. Alibakhshikenari, B. S. Virdee, O. Abdullah, S. Khan, P. Livreri, A. Al-Jumaily, M. F. A. Sree, *et al.*, "AI-based investigation and mitigation of rain effect on channel performance with aid of a novel 3D slot array antenna design for high throughput satellite system," *IEEE Access*, Vol. 12, 29 926–29 939, 2024.

[5] Al-Adhami, A., Y. Al-Adhami, and T. A. Elwi, "A 3D antenna array based solar cell integration for modern MIMO systems," *Infocommunications Journal*, Vol. XV, No. 4, 10–16, Dec. 2023.

[6] Jwair, M. H., T. A. Elwi, S. K. Khamas, A. Farajidavar, and A. B. Ismail, "Circularly shaped metamaterial fractal reconfigurable antenna for 5G networks," *Iraqi Journal of Information and Communication Technology*, Vol. 6, No. 3, 65–75, 2023.

[7] Abood, M. S., H. Wang, D. He, M. Fathy, S. A. Rashid, M. Alibakhshikenari, B. S. Virdee, S. Khan, G. Pau, I. Dayoub, *et al.*, "An LSTM-based network slicing classification future predictive framework for optimized resource allocation in C-V2X," *IEEE Access*, Vol. 11, 129 300–129 310, 2023.

[8] Abdulsattar, R. K., S. M. Sadeq, T. A. Elwi, Z. A. A. Hassain, and M. Y. Muhsin, "Artificial neural network approach for estimation of moisture content in crude oil by using a microwave sensor," *International Journal of Microwave & Optical Technology*, Vol. 18, No. 5, 511–519, 2023.

[9] Jwair, M. H., T. A. Elwi, M. Alibakhshikenari, B. S. Virdee, H. Almizan, Z. A. A. Hassain, S. M. Ali, L. Kouhalvandi, P. Livreri, N. T. Tokan, *et al.*, "Intelligent metasurface layer for direct antenna amplitude modulation scheme," *IEEE Access*, Vol. 11, 77 506–77 517, 2023.

[10] Ismail, M. M., T. A. Elwi, and A. J. Salim, "Design and simulation of a CRLH transmission line antenna of a Hilbert fractal geometry for S-band appications," in *2021 International Conference on Electrical, Computer and Energy Technologies (ICECET)*, 1–5, Cape Town, South Africa, 2021.

[11] Hussein, H., F. Atasoy, and T. Elwi, "Origami antenna array shaped Mosque of Muhammad Al-Fatih for visual sight enhancement in modren 5G MIMO networks," *Journal of Engineering and Sustainable Development*, Vol. 27, No. 4, 417–428, 2023.

[12] Ali, L., M. Ilyas, and T. A. Elwi, "A metamaterial-based compact MIMO antenna array incorporating Hilbert fractal design for enhanced 5G wireless communication networks," *Mathematical Modelling of Engineering Problems*, Vol. 10, No. 3, 930–936, 2023.

[13] Muqdad, Z. S., F. Taher, T. A. Elwi, Z. A. A. Hassain, M. Alibakhshikenari, M. F. A. Sree, M. I. Ibrahem, M. Alsabaan, B. S. Virdee, P. Livreri, and E. Limiti, "Breast cancer detection using a modern microwave technique based neural network algorithms for medical applications," *International Journal of Microwave and Wireless Technologies*, Vol. 16, No. 4, 345–360, 2024.

[14] Hassain, Z. A. A., M. J. Farhan, T. A. Elwi, and I. A. Mocanu, "Design and optimization of an inductive-stub-coupled CSRR for non-invasive glucose sensing," *Sensors*, Vol. 24, No. 24, 7592, 2024.

[15] Jwair, M. H. and T. A. Elwi, "Metasurface antenna circuitry for 5G communication networks," *Infocommunications Journal*, No. 2, 2–7, 2023.

[16] Alibakhshikenari, M., B. S. Virdee, T. A. Elwi, I. D. Lubangakene, R. K. R. Jayanthi, A. A. Al-Behadili, Z. A. A. Hassain, S. M. Ali, G. Pau, P. Livreri, and S. Aïssa, "Design of a planar sensor based on split-ring resonators for non-invasive permittivity measurement," *Sensors*, Vol. 23, No. 11, 5306, 2023.

[17] Abdulsattar, R. K., M. Alibakhshikenari, B. S. Virdee, R. Sharma, T. A. Elwi, L. Kouhalvandi, Z. A. A. Hassain, S. M. Ali, N. T. Tokan, P. Livreri, F. Falcone, and E. Limiti, "Optical-microwave sensor for real-time measurement of water contamination in oil derivatives," *AEU — International Journal of Electronics and Communications*, Vol. 170, 154798, 2023.

[18] Hussein, H., F. Atasoy, and T. A. Elwi, "Miniaturized antenna array-based novel metamaterial technology for reconfigurable MIMO systems," *Sensors*, Vol. 23, No. 13, 5871, 2023.

[19] Soni, G. K., D. Yadav, A. Kumar, P. Jain, and A. Rathi, "Design and SAR analysis of DGS based deformed microstrip antenna for ON/OFF body smart wearable IoT applications," *Physica Scripta*, Vol. 100, No. 1, 015536, 2024.

[20] Jain, P., P. K. Sahoo, A. D. Khaleel, and A. J. A. Al-Gburi, "Enhanced prediction of metamaterial antenna parameters using advanced machine learning regression models," *Progress In Electromagnetics Research C*, Vol. 146, 1–12, 2024.

[21] Soni, G. K., D. Yadav, A. Kumar, P. Jain, and M. V. Yadav, "Design and optimization of flexible DGS-based microstrip antenna for wearable devices in the sub-6 GHz range using the Nelder-Mead simplex algorithm," *Results in Engineering*,

Vol. 24, 103470, 2024.

[22] Thella, R. K., A. Sabah, J. Kumar, M. A. Al-Janabi, T. A. Oleiwi, and S. Peddakrishna, "E-shaped inspired 2.4 GHz compact microstrip patch antenna," in *Proceedings of the 2024 4th International Conference on Artificial Intelligence and Signal Processing (AISP)*, 1–4, Vijayawada, India, 2024.

[23] Ismail, M. M., B. B. Q. Elias, B. S. Bashar, T. A. Elwi, Z. A. Rhazali, and H. Misran, "Frequency reconfigurable using CLRH for 5G sub-6 GHz wireless application," *Iraqi Journal of Information and Communication Technology*, Vol. 8, No. 3, 62–72, 2025.

[24] Marhoon, H. M., A. I. Alanssari, and N. Basil, "Design and implementation of an intelligent safety and security system for vehicles based on GSM communication and IoT network for real-time tracking," *Journal of Robotics and Control (JRC)*, Vol. 4, No. 5, 708–718, 2023.

[25] Feng, B., X. He, J.-C. Cheng, Q. Zeng, and C.-Y.-D. Sim, "A low-profile differentially fed dual-polarized antenna with high gain and isolation for 5G microcell communications," *IEEE Transactions on Antennas and Propagation*, Vol. 68, No. 1, 90–99, 2020.

[26] Verma, A., R. K. Arya, R. Bhattacharya, and S. N. Raghava, "Compact PIFA antenna with high gain and low SAR using AMC for WLAN/C-band/5G applications," *IETE Journal of Research*, Vol. 69, No. 7, 4422–4432, 2023.

[27] Liu, Q., H. Liu, W. He, and S. He, "A low-profile dual-band dual-polarized antenna with an AMC reflector for 5G communications," *IEEE Access*, Vol. 8, 24 072–24 080, 2020.

[28] Ashish, J. and A. P. Rao, "A dual band AMC backed antenna for WLAN, WiMAX and 5G wireless applications," *Applied Computational Electromagnetics Society Journal (ACES)*, Vol. 36, No. 9, 1209–1214, 2021.

[29] Malekpoor, H., A. Abolmasoumi, and M. Hamidkhani, "High gain, high isolation, and low-profile two-element MIMO array loaded by the Giuseppe Peano AMC reflector for wireless communication systems," *IET Microwaves, Antennas & Propagation*, Vol. 16, No. 1, 46–61, 2022.

[30] Al-Asady, R., T. A. Elwi, and B. Ruthramurthy, "A modern RIS design based AI driven for cooperative relay networks," *Iraqi Journal of Information and Communication Technology*, Vol. 8, No. 3, 73–82, 2025.

[31] Shabeeb Kamil, A., E. M. Ali, M. Alibakhshikenari, N. Misran, M. T. Islam, B. Virdee, D. Mariyanayagam, N. A. Abbasi, N. Rashid, and T. A. Elwi, "Metasurface effect on the performance of planar antennas for wireless communications," *Radio Science*, Vol. 60, No. 11, e2024RS008156, 2025.

[32] Kamil, R. A., S. M. B. Alsabti, R. K. Abdulsattar, A. H. Mohammed, and T. A. Elwi, "On the enhancement anomaly detection for RF bio-sensors by computing artificial networks using machine learning techniques," *Infocommunications Journal*, Vol. 17, No. 2, 89–95, 2025.